Graphene Cathode-Based ZnO Nanowire Hybrid Solar Cells

Hyesung Park,[†,‡,⊥] Sehoon Chang,[‡,⊥] Joel Jean,[†] Jayce J. Cheng,[‡] Paulo T. Araujo,[†] Mingsheng Wang,[‡] Moungi G. Bawendi,[§] Mildred S. Dresselhaus,[†,∥] Vladimir Bulović,[†] Jing Kong,[†] and Silvija Gradečak*,[‡]

[†]Department of Electrical Engineering and Computer Science, Massachusetts Institute of Technology, Cambridge, Massachusetts 02139, United States

[‡]Department of Materials Science and Engineering, Massachusetts Institute of Technology, Cambridge, Massachusetts, 02139, United States

[§]Department of Chemistry, Massachusetts Institute of Technology, Cambridge, Massachusetts, 02139, United States

[∥]Department of Physics, Massachusetts Institute of Technology, Cambridge, Massachusetts, 02139, United States

Ⓢ Supporting Information

ABSTRACT: Growth of semiconducting nanostructures on graphene would open up opportunities for the development of flexible optoelectronic devices, but challenges remain in preserving the structural and electrical properties of graphene during this process. We demonstrate growth of highly uniform and well-aligned ZnO nanowire arrays on graphene by modifying the graphene surface with conductive polymer interlayers. On the basis of this structure, we then demonstrate graphene cathode-based hybrid solar cells using two different photoactive materials, PbS quantum dots and the conjugated polymer P3HT, with AM 1.5G power conversion efficiencies of 4.2% and 0.5%, respectively, approaching the performance of ITO-based devices with similar architectures. Our method preserves beneficial properties of graphene and demonstrates that it can serve as a viable replacement for ITO in various photovoltaic device configurations.

KEYWORDS: graphene, ZnO nanowires, solar cells, ITO
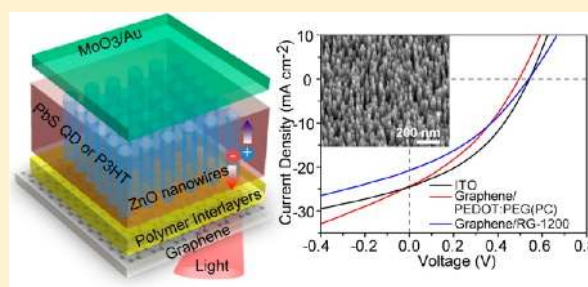
The recent discovery[1] and successful large-area synthesis[2,3] of graphene, with its unique physical properties,[4−7] have led to a growing interest in its application for optoelectronic devices such as solar cells and light-emitting diodes.[8−13] Because of its high transparency and electrical conductivity, chemical and mechanical robustness, as well as materials abundance, graphene is being explored as a potential replacement for indium tin oxide (ITO) as a transparent conducting electrode material.[14,15] Simultaneously with the graphene development, single-crystalline semiconducting nanowires have been widely investigated due to their novel electrical and optical properties.[16] In particular, nanowire-based hybrid photovoltaic (PV) structures have gained significant interest because of their potential to achieve efficient charge extraction via one-dimensional charge transport pathways and large interfacial area in well-ordered bulk heterojunction geometry.[17,18] Combining the properties of graphene and semiconducting nanowires would thus provide a unique platform for the development of nanostructured solar cells with superior transparency and flexibility as well as improved stability.

The growth of single-crystalline semiconducting nanowires for optoelectronic applications has been demonstrated by a variety of growth techniques, including metalorganic vapor phase epitaxy (MOVPE), molecular beam epitaxy, and solution-based hydrothermal processes. These methods enable direct growth of nanowires on various conductive substrates

such as aluminum foil or ITO, as well as on cost-effective flexible substrates. However, growing 1D semiconducting nanostructures directly on pristine graphene without impairing its electrical and structural properties has been challenging due to graphene's stable and inert sp²-hybridized structure. High temperature (∼400 °C) MOVPE growth of ZnO nanowires on graphene has recently been demonstrated,[19] but this process requires destructive oxygen plasma treatment of the graphene substrate to break the sp²-hybridized graphene surface[20] and generate step edges that act as ZnO nanowire nucleation sites. The growth of ZnO nanorods on graphene by a hydrothermal method has also been suggested,[21] but no hydrothermally grown nanorod/graphene-based optoelectronic devices have been demonstrated, thus leaving an open question about the structural and electrical integrity of the graphene during this process. Obtaining an effective interface between nanowires and graphene while maintaining the advantages of each component will therefore play a critical role in future applications of this materials system.

To address these challenges, we report a simple method to grow high-quality ZnO nanowires on graphene via the

hydrothermal method.[22−24] We focus on ZnO nanowires because of their low-temperature processability over a large area, structural robustness, and excellent lattice-matching with graphene.[25] Our method is enabled by an interfacial modification that preserves the structural and electrical properties of both the nanowires and the graphene. We then demonstrate graphene cathode-based hybrid solar cells by using two different solution-processed photoactive materials, PbS quantum dots (QDs) and poly(3-hexylthiophene) (P3HT) conjugated polymers, and ZnO nanowires as hole and electron transport layers, respectively. The performance of ZnO nanowire/graphene-based solar cells approaches that of ITO-based devices with similar architectures.

In this work, ZnO nanowires were grown via a hydrothermal method on graphene and, for comparison, on ITO substrates, and both architectures were used for subsequent device fabrication and testing (for more details, see Methods section and Supporting Information Figure S1). Graphene sheets were synthesized via low-pressure chemical vapor deposition and the graphene electrodes were fabricated through a layer-by-layer transfer method by stacking three monolayers of graphene films[9] (Figure 1a). The resulting average sheet resistance and
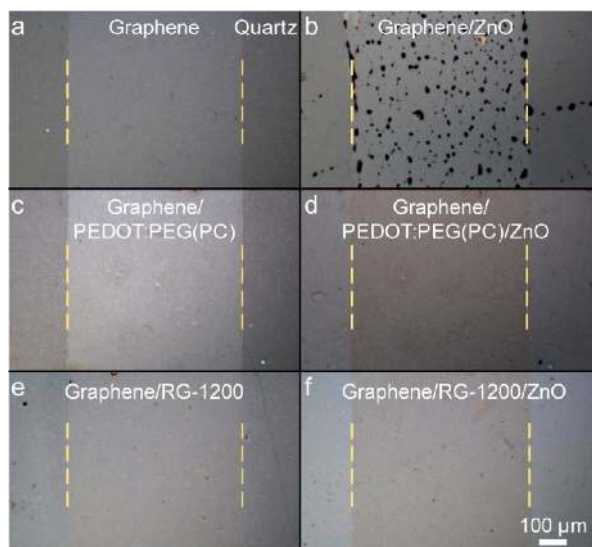
Figure 1. ZnO seed layer wetting properties on the modified graphene substrates. Bright-field optical microscopy images of (a) graphene strip on a quartz substrate, (b) ZnO seed layer spin-coated on pristine graphene showing dewetting of the ZnO film to form islands, (c,d) graphene/PEDOT:PEG(PC) before and after the ZnO seed layer deposition, respectively, and (e,f) graphene/RG-1200 before and after the ZnO seed layer deposition, respectively. Parts c−f illustrate uniform coverage of both polymers on the graphene surface and of the ZnO seed layer on the modified graphene.

transmittance values were 300 ± 12 $\Omega/\square$ and $92.0 \pm 0.4\%$ (at $\lambda = 550$ nm), respectively, similar to those reported elsewhere.[14] A critical step for the hydrothermal growth of ZnO nanowires is the deposition of a uniform, high-quality ZnO seed layer, which we obtain by annealing a layer of zinc acetate dihydrate in 2-methoxyethanol spin-coated on the growth substrate (see Methods section). In the case of ITO, this process yields a uniform ZnO film. On a pristine graphene surface, however, the low surface free energy[26] and the hydrophobic nature of graphene[9] result in poor wetting by the ZnO seed layer and the formation of dewetted ZnO islands

(Figure 1b and Supporting Information Figure S2). Similar poor wetting of graphene has been reported with other material systems, such as poly(3,4-ethylenedioxythiophene):poly-(styrenesulfonate) (PEDOT:PSS) in aqueous solution, which is commonly used as a hole injection layer. It is therefore desirable to develop a nondestructive method to modify the graphene surface that enables uniform deposition of the ZnO seed layer.

Here, we modified the graphene surface with conducting polymers that (1) wet the graphene surface, (2) provide a more chemically compatible surface with the subsequent ZnO layer, and (3) enable charge transfer between the ZnO and the graphene. Two commercially available conducting polymers, poly(3,4-ethylenedioxythiophene)-block-poly(ethylene glycol) (PEDOT:PEG) doped with perchlorate (PC) in nitromethane and sulfonated poly(thiophene-3-[2-(2-methoxyethoxy)-ethoxy]-2,5-diyl) (Plexcore OC RG-1200) in ethylene glycol monobutyl ether/water (3:2), which we refer to as PEDOT:PEG(PC) and RG-1200, respectively, were used as interfacial layers, spin-coated onto graphene prior to ZnO seed layer deposition. These polymers are dissolved in solvents (nitromethane and ethylene glycol monobutyl ether) with good wetting properties on the graphene surface, and the surface modification of graphene with both conducting polymers enables uniform deposition of the ZnO films (Figure 1c−f).

The growth of uniform and ordered ZnO nanowire arrays is highly dependent on the uniformity of the ZnO seed layer, which is in turn strongly affected by the annealing temper-ature[22] and ambient conditions (Supporting Information Figure S3). Therefore, we next considered the effect of the interfacial layer on the uniformity of the ZnO seed layer and the resulting nanowire quality. The ZnO seed layer is obtained by thermal decomposition of zinc acetate dihydrate (see Methods) at temperatures above the solid sublimation temperature (~175 °C). Because a full transformation to ZnO occurs at 335 °C,[22] annealing conditions are typically selected to be in the 175—335 °C temperature range. Annealing the polymeric interlayers above their thermal degradation temperature (e.g., ~235 °C for PEDOT[28]) can affect their morphology and conductivity. When ZnO seed layers on PEDOT were annealed at temperatures above 235 °C, the uniformity and morphology of the resulting ZnO nanowire arrays were significantly altered due to wrinkling of the underlying polymer (Supporting Information Figure S4). Hence, we limited the annealing temperature of the seed layer below this critical value to maintain the structural integrity and potentially the electrical properties of the polymeric interlayer as well as the quality of the ZnO nanowire arrays.

In addition to the annealing temperature, the choice of interfacial polymer can affect the morphology of the ZnO seed layer. To characterize any morphological changes, the surface of ZnO films on the modified graphene surfaces and on ITO for comparison was investigated by atomic force microscopy (AFM). Acetate-derived ZnO seed layers on ITO are uniform and smooth, with a root-mean-square (rms) roughness of less than 2 nm (Figure 2a), and yield well-ordered ZnO nanowire arrays (Figure 3a). The surface of pristine graphene (Figure 2b) after deposition of PEDOT:PEG(PC) shows a rms roughness of 34 nm (Figure 2c), which decreases to 24 nm after the deposition of a conformal ZnO seed layer (Figure 2d). Similar trends were observed for graphene films modified with RG-1200, but the surface was smoother than in the case of PEDOT:PEG(PC), with measured rms roughness values for
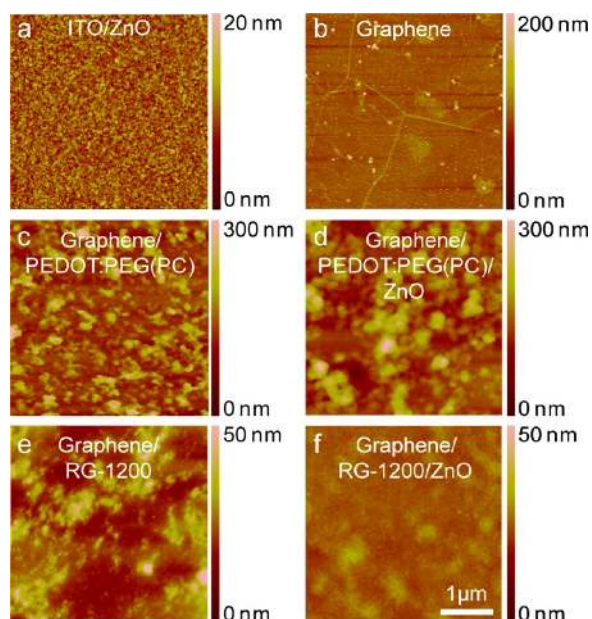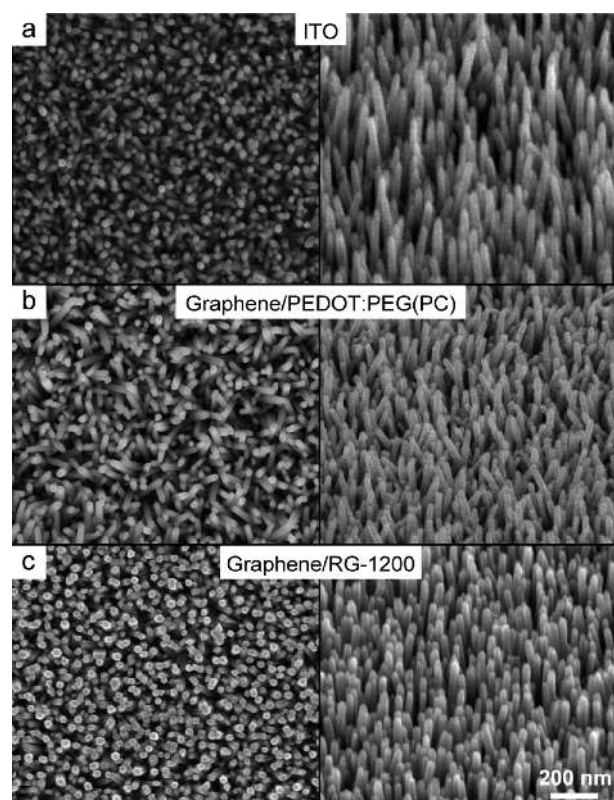
Figure 2. Surface morphology analysis of ZnO seed layers on graphene transferred on ITO and graphene substrates. Tapping mode AFM images of (a) ITO/ZnO, (b) graphene, (c,d) graphene/PEDOT:PEG-(PC) before and after the ZnO seed deposition, respectively, (e,f) graphene/RG-1200 before and after the ZnO seed deposition, respectively. Both polymers completely coat the graphene surface (c,e) and ZnO conformally covers the underlying polymers (d,f). In addition, surfaces of both polymers are smoothed upon deposition of ZnO layers: the rms roughness is reduced from 34 to 25 nm for PEDOT:PEG(PC) and from 6 to 2 nm for RG-1200.

Figure 3. SEM characterization of ZnO nanowire arrays grown on ITO and on graphene modified with polymer interfacial layers. Hydrothermally grown ZnO nanowire arrays on (a) ITO substrates, (b) graphene/PEDOT:PEG(PC), and (c) graphene/RG-1200. ZnO nanowire arrays grown under the same experimental conditions on ITO and modified graphene show similar uniformity and alignment.

graphene/RG-1200 and graphene/RG-1200/ZnO of 6 and 2 nm, respectively (Figure 2d,e). Figure 3 shows scanning electron microscopy (SEM) images of ZnO nanowire arrays grown on ITO and on modified graphene under identical conditions. Notably, the morphology of nanowires grown on the modified graphene substrates is comparable to that obtained on ITO. ZnO nanowire arrays grown on a graphene/RG-1200 substrate exhibit better nanowire alignment (order parameter $S_{RG-1200} = 0.992$) than those on a graphene/PEDOT:PEG(PC) substrate ($S_{PEDOT:PEG(PC)} = 0.938$) and similar alignment to arrays grown on ITO ($S_{ITO} = 0.997$), corroborating the idea that the roughness of the ZnO seed layer affects the alignment of the nanowire arrays. For both polymers, ZnO nanowires grown under identical conditions were approximately 400 nm long and with an average diameter of 20 nm.

To assess the structural and optical quality of as-grown ZnO nanowires on graphene, we performed transmission electron microscopy (TEM) and photoluminescence (PL) measurements (Figure 4). Strong near band edge emission at 376 nm, as well as a relatively weak defect peak centered at 550−600 nm that is typically associated with singly ionized oxygen defects in ZnO nanowires, both confirm the excellent quality of ZnO nanowires grown on graphene. High-resolution TEM images of ZnO nanowires grown on graphene with polymer interlayers show the well-resolved lattice with a spacing of ∼0.52 nm in the [0001] growth direction.

The above results demonstrate the broad applicability of our proposed approach for growing well-ordered ZnO nanowires on a graphene surface via nondestructive modification with conductive polymeric interlayers. To elucidate possible

interactions, such as doping via charge transfer, between graphene, the polymer interlayer (PEDOT:PEG(PC)), and the ZnO seed layer, we performed resonant Raman spectroscopy analysis as a fast and nondestructive technique that has been extensively used to study structural changes and the effect of doping in polymers such as PEDOT or PEDOT:PSS, as well as in graphene.[29−31] Figure 5a shows the Raman spectra of PEDOT:PEG(PC) and PEDOT:PEG(PC)/ZnO samples within the frequency range that corresponds to carbon−carbon (C−C and C=C) stretch vibrations in the benzoid/quinoid structure present in a typical PEDOT system.[29−31] The Raman spectra were fitted with Lorentzian curves, and the resulting fitting parameters are summarized in Table 1. The strongest feature in the Raman spectrum of PEDOT:PEG(PC) is a peak centered at 1441 cm^{-1} (P1) that can be attributed to in-plane stretching of the C=C double bonds. The frequency of this Raman peak is known to be sensitive to the negative (reduction) and positive (oxidation) doping of the polymer; namely, reduction (oxidation) result in both a frequency red (blue) shift and linewidth narrowing (broadening).[29−31] Because of this sensitivity, we used peak P1 to investigate the potential interactions between PEDOT:PEG(PC), ZnO, and graphene. The peak P1 frequency for PEDOT:PEG(PC)/ZnO system is red-shifted by 6 cm^{-1} relative to that of pristine PEDOT:PEG(PC), while the respective spectral linewidth narrows by 6 cm^{-1}. Comparison of our Raman results with previously reported peak shifts and linewidth changes as a function of PEDOT:PSS doping[29−31] indicate that the polymer
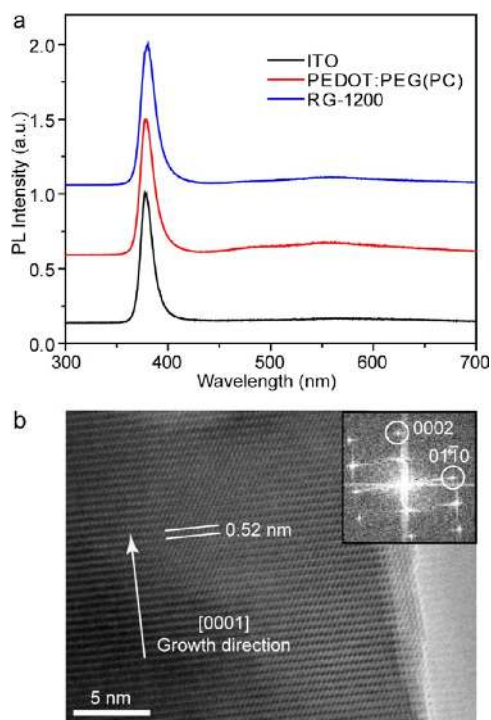
Figure 4. Optical and structural characterization of ZnO nanowires on graphene. (a) PL spectra of ZnO nanowires grown on ITO, graphene/PEDOT:PEG(PC), and graphene/RG-1200. In all cases, the low PL intensity of the broad 550 nm peak confirms a low defect density related to hydroxyl groups and strong near-band-edge luminescence centered at 376 nm confirms the structural quality of the ZnO nanowires. (b) High-resolution TEM image and the corresponding Fourier transform (inset) show the single-crystalline wurtzite structure of ZnO nanowires, with a lattice spacing of 0.52 nm in the [0001] growth direction.

is reduced when in contact with ZnO. In contrast, when the PEDOT:PEG(PC) layer is in contact with graphene, peak P1

Table 1. Frequency (ω) and Spectral Linewidth (γ) of Raman Peak P1, Obtained by Fitting the Spectra in Figure 5

sample	ω (cm^{-1})	γ (cm^{-1})
PEDOT:PEG(PC)	1441	42
PEDOT:PEG(PC)/ZnO	1435	36
graphene/PEDOT:PEG(PC)	1445	48
graphene/PEDOT:PEG(PC)/ZnO	1439	38

blue-shifts by 4 cm^{-1} and its spectral linewidth broadens by 6 cm^{-1} relative to that of the pristine graphene, indicating oxidation of the PEDOT:PEG(PC) (Figure 5b). Finally, by measuring the P1 peak of the final graphene/PEDOT:PEG-(PC)/ZnO system (Figure 5c), we observe that its frequency is red-shifted by 2 cm^{-1} and the linewidth narrows by 4 cm^{-1} relative to that of pristine PEDOT:PEG(PC). This finding is in agreement with our results on the individual two-component systems (graphene/PEDOT:PEG(PC) and PEDOT:PEG-(PC)/ZnO)) because the reduction of the polymer caused by ZnO is more prominent than the oxidation caused by graphene. From these observations, we expect electrons to transfer from ZnO to the conducting polymer PEDOT:PEG(PC) and ultimately to the graphene electrodes, as desired in a full device configuration.

After obtaining uniform arrays of ZnO nanowires on graphene, we fabricated graphene cathode-based hybrid solar cells using PbS QDs[32] and P3HT as p-type hole-transporting donor materials and the ZnO nanowires as electron-transporting channels to the cathode. The as-grown graphene/ZnO nanowire structure is well-suited for an inverted device geometry, which offers improved stability over conventional ITO anode-based geometries by avoiding an acidic PEDOT:PSS layer and easily oxidized low work function metals (e.g., Al or Ag).[33]

For both types of devices, prior to ZnO nanowire growth, graphene electrodes were treated with polymeric interlayers, whereas ITO electrodes were treated with oxygen plasma. Detailed fabrication and testing procedures are described in the
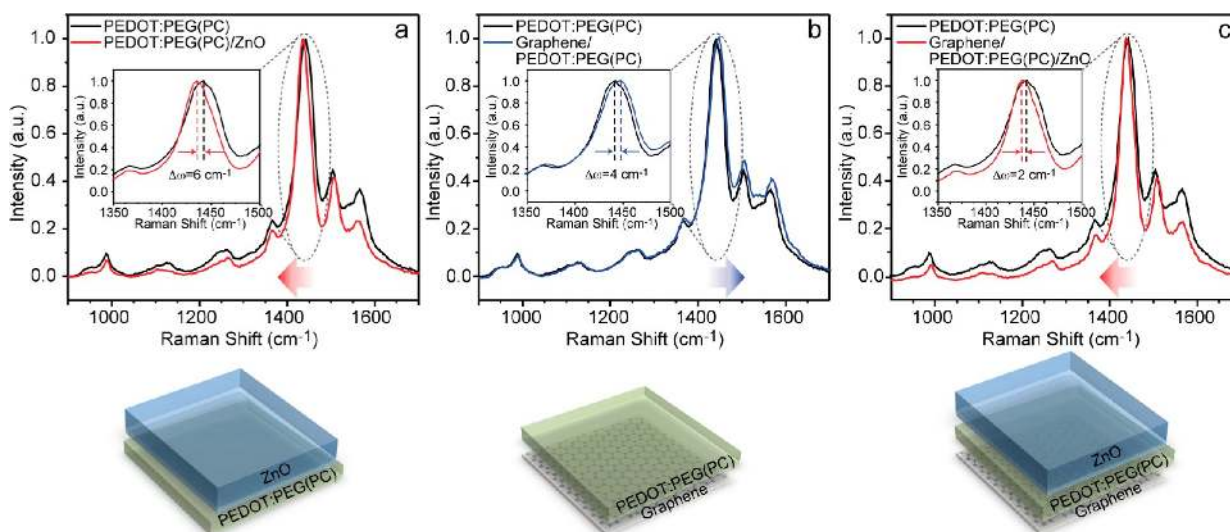
Figure 5. Raman analysis of PEDOT:PEG(PC) polymer and its hybrid counterparts. (a) Raman spectra of the PEDOT:PEG(PC) and PEDOT:PEG(PC)/ZnO with the peak P1 centered at 1441 cm^{-1}. The polymer is reduced upon interaction with ZnO, as evidenced by a decrease in frequency (red-shift by 6 cm^{-1}) at 1441 cm^{-1}. (b) Raman peak P1 is blue-shifted by 4 cm^{-1} when in contact with graphene. (c) Raman peak P1 is red-shifted by 2 cm^{-1} in the full graphene/PEDOT:PEG(PC)/ZnO system. In all of these plots, the intensities were normalized to their maximum values to compare the spectral features.

Methods section. Figures 6a,b show the overall device structure and the corresponding flat-band energy level diagram. Cross-
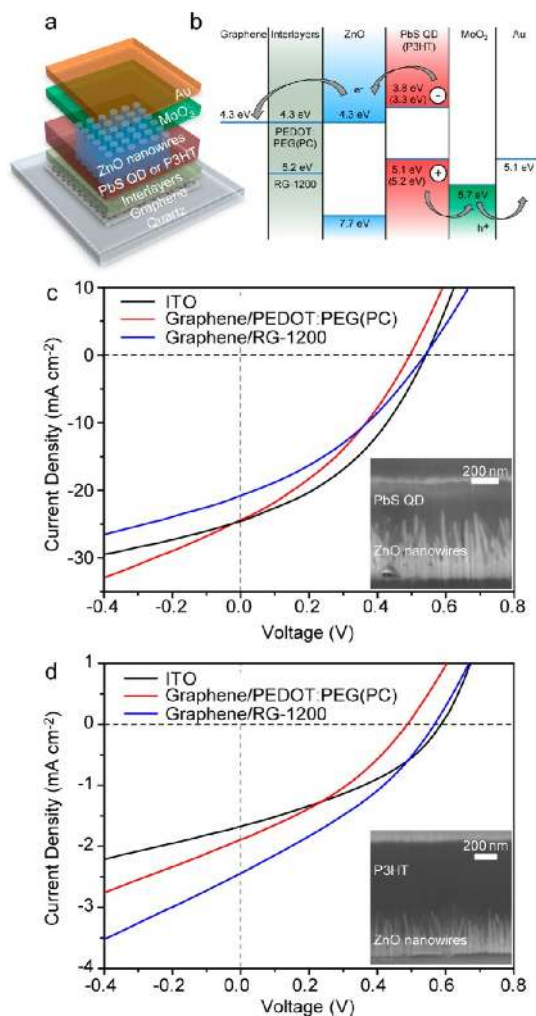
Figure 6. Hybrid graphene/ZnO nanowire solar cells. (a) Schematic diagram of the graphene cathode hybrid solar cells: graphene deposited on quartz is covered by a polymer (PEDOT:PEG(PC) or RG-1200), followed by the ZnO seed layer and 400 nm long ZnO nanowires. The nanowires are then infiltrated and covered with PbS QDs (300 nm) or P3HT (700 nm) and finally with MoO_3 (25 nm)/ Au (100 nm) top electrodes. (b) Flat-band energy level diagram of the solar cells shown in (a). (c) $J-V$ characteristics under 100 mW/cm² AM1.5G illumination of the champion graphene-based PbS QD device with different polymer interlayers, demonstrating performance comparable to that of an ITO reference cell. (d) $J-V$ characteristics of representative graphene-based P3HT devices with different polymer interlayers, compared with an ITO reference device. Insets in (c) and (d) show SEM cross-section images of the complete devices, showing substantial infiltration of the photoactive materials (PbS QD or P3HT) into the nanometer-scale gaps between ZnO nanowires.

sectional SEM images (Figure 6c,d insets) show that the PbS QDs and P3HT infiltrate deep into the ZnO nanowire arrays, as is critical for efficient charge separation.[32] Figures 6c,d compare representative current density–voltage ($J-V$) characteristics under AM1.5G illumination at 100 mW/cm² of solar cells with graphene and ITO electrodes. With optimized ZnO nanowire growth conditions, we observed efficient device performance for both ITO and graphene electrodes in both device architectures: the power conversion efficiency (PCE) of

PbS QD-based devices was 5.1% for ITO/ZnO, 4.2% for graphene/PEDOT:PEG(PC)/ZnO, and 3.9% for graphene/ RG-1200/ZnO; the corresponding PCEs for P3HT-based devices were 0.4%, 0.3%, and 0.5%, respectively. The primary photovoltaic performance parameters are summarized in Table 2.

Our results constitute the first demonstration of graphene-based hybrid photovoltaic devices employing ZnO nanowires in an inverted configuration. With graphene electrodes consisting of only three stacked monolayers, the observed device performance approaches that of ITO-based solar cells. Furthermore, for the ZnO nanowire-based P3HT architecture, the efficiencies achieved in this work equal or exceed those reported previously for similar ITO-based devices.[34,35] These results indicate that the proposed substrate-independent method for polymeric interfacial modification enables the growth of high-quality and ordered ZnO nanowire arrays on graphene while preserving its electrical and structural properties. Our nondestructive and substrate-independent approach is favorable for processing graphene without causing significant damage, in contrast to destructive physical etching.

In conclusion, highly uniform, well-aligned ZnO nanowire arrays were successfully grown on graphene via a hydrothermal method. This growth was enabled by a simple interfacial polymer treatment that facilitates conformal, smooth wetting of the ZnO seed layer and subsequent ordered nanowire growth. Using ZnO nanowires as an electron transport layer, graphene cathode-based inverted solar cells were fabricated with PCEs of 4.2% and 0.5% for PbS quantum dot and P3HT devices, respectively, comparable to the performance of equivalent ITO-based devices. Our work suggests that graphene could serve as a viable alternative to ITO in various photovoltaic device configurations. The simple method reported herein for fabricating semiconducting nanostructures on graphene via interface engineering preserves its structural and electrical properties, and hence may be applicable to a variety of nanoelectronic devices.

Methods. *Graphene Synthesis and Transfer.* Graphene films were synthesized via low pressure chemical vapor deposition using copper foil (25 μm in thickness, ALFA AESAR) as a metal catalyst. The growth chamber was evacuated to a base pressure of 30−50 mTorr, heated to a growth temperature of 1000 °C under hydrogen gas (H_2, 10 sccm, ∼320 mTorr), and annealed for 30 min. Subsequently, methane gas (CH_4, 20 sccm, total pressure: ∼810 mTorr) was introduced and graphene growth was carried out for 30 min. The chamber was then cooled down at ∼45 °C/min to room temperature. Transfer of graphene from the growth substrate was performed using poly(methyl methacrylate) (PMMA, 950 A9, Microchem). Graphene on one side of the Cu foil was removed via reactive ion etching with oxygen gas (Plasma-Therm, 100 W at 7×10^{-5} Torr) before the Cu was etched away (Cu etchant: CE-100, Transene). Graphene films were then thoroughly rinsed with hydrochloric acid (10%) and deionized (DI) water. Finally, the PMMA layer was removed by annealing at 500 °C for 2 h under H_2 (700 sccm) and Ar (400 sccm). Repeated transfers were performed to form three-layer graphene stacks.

Polymer Interfacial Layers. PEDOT:PEG(PC) (Sigma Aldrich) in nitromethane was filtered (0.2 μm), spin-coated in air at 5000 rpm for 60 s, and spin-dried in air. Plexcore OC RG-1200 (Sigma Aldrich) in ethylene glycol monobutyl ether/

Table 2. Summary of Photovoltaic Performance Parameters of Graphene- and ITO-Based Devices, Indicating Champion and Average Values

cathode	interface layer	hole transport layer	J_{SC} (mA/cm^2)	V_{OC} (V)	FF (%)	PCE (%)
ITO		PbS QD	24.6 (24.3 ± 0.3)	0.54 (0.49 ± 0.04)	38.6 (36.3 ± 1.6)	5.1 (4.4 ± 0.6)
graphene	PEDOT:PEG(PC)	PbS QD	24.4 (22.5 ± 1.3)	0.50 (0.49 ± 0.01)	34.6 (34.4 ± 0.3)	4.2 (3.8 ± 0.3)
graphene	RG-1200	PbS QD	20.8 (18.5 ± 1.9)	0.54 (0.54 ± 0.01)	34.9 (33.3 ± 3.2)	3.9 (3.3 ± 0.6)
ITO		P3HT	1.7 (1.6 ± 0.1)	0.59 (0.56 ± 0.04)	36.8 (35.3 ± 1.8)	0.4 (0.3 ± 0.1)
graphene	PEDOT:PEG(PC)	P3HT	1.9 (1.6 ± 0.2)	0.49 (0.46 ± 0.04)	33.8 (32.2 ± 2.0)	0.3 (0.2 ± 0.1)
graphene	RG-1200	P3HT	2.4 (1.9 ± 0.5)	0.57 (0.50 ± 0.06)	32.9 (29.8 ± 2.7)	0.5 (0.3 ± 0.1)

water (3:2) was filtered (0.45 μm), spin-coated in air at 4000 rpm for 60 s, and annealed at 175 °C for 30 min in air.

ZnO Nanowires Growth. ZnO nanowires were grown on PEDOT:PEG(PC) or RG-1200 by a hydrothermal method. ZnO seed layers were prepared by spin-coating 300 mM of zinc acetate dihydrate and ethanolamine in 2-methoxyethanol solution and annealing at 175 °C for 10 min. This process was repeated twice to form a uniform ZnO seed layer on PEDOT:PEG(PC) or RG-1200. The substrate was subsequently immersed into the nanowire growth solution for 40 min at 90 °C. The growth solution consisted of 50 mM zinc nitrate hexahydrate (25 mL) and 50 mM hexamethylenetetramine (25 mL) in DI water. As-grown ZnO nanowires were thoroughly rinsed in DI water and annealed at 200 °C for 5 min to remove residual DI water.

Structural Characterization. The surface morphologies of graphene, PEDOT:PEG(PC), RG-1200, and ZnO seed layers were characterized using a Digital Instruments Veeco Dimension 3100 atomic force microscope operated in tapping mode. Scanning electron microscopy was performed with a Helios Nanolab 600 at 5 kV. Transmission electron microscopy (TEM) images, and the corresponding electron diffraction patterns of as-prepared ZnO samples were obtained using a JEOL 2010F with an accelerating voltage of 200 kV.

Raman and Optical Analysis. Raman spectra were taken with a 532 nm wavelength laser source (Nd:YAG laser) in the backscattering geometry using a 100× objective. The laser power measured from the objective was 1.5 mW. PL measurement of the as-grown ZnO nanowires on seeded Si substrates was conducted at room temperature, with a laser operating at 262 nm and a power density of 60 W/cm^2.

Device Fabrication. Prepatterned ITO substrates (Thin Film Devices, 150 nm thick, 20 Ω/sq, 85%T) were cleaned by sonication in soap water (Micro-90, Cole-Parmer), DI water, acetone, and isopropyl alcohol, followed by oxygen plasma cleaning (100 W, Plasma Preen, Inc.) for 30 s. Patterned graphene substrates were cleaned by annealing at 500 °C for 30 min under H$_2$ (700 sccm) and Ar (400 sccm).

ZnO-Nanowire/P3HT Hybrid Solar Cells. A solution of poly(3-hexylthiophene-2,5-diyl) (P3HT, Plexcore OS 2100) in 1,2-dichlorobenzene (30 mg/mL) was prepared. Cyclohexanone (10 vol%) was then added into the P3HT solution, and the solution turned purple after 24 h, indicative of P3HT nanofiber formation. The polymer solution was spin-coated on ZnO nanowire arrays at 1000 rpm for 60 s in a nitrogen-filled glovebox. The substrates were annealed at 150 °C inside the glovebox for 45 min to ensure the infiltration of P3HT nanofibers into the voids of nanowire arrays. MoO$_3$ (Alfa Aesar, 99.9995%) and the top anode Au (Kurt J. Lesker, 3.175 mm pallets, 99.999%) were thermally evaporated through shadow masks at a base pressure of 2 × 10^{-6} Torr at rates of 1.0 and 1.5

Å/s, respectively. The device area defined by the overlap between the top and bottom electrodes was 1.21 mm^2.

ZnO-Nanowire/PbS QD Hybrid Solar Cells. Colloidal PbS QDs with the first excitonic peak at 905 nm (1.36 eV) were synthesized according to literature[36] methods and deposited on ZnO nanowire by sequential layer-by-layer spin-casting, as reported elsewhere.[32] Each spin-casting cycle deposited ~30 nm of QDs, with a typical film thickness of ~300 nm achieved through 10 deposition cycles. A 25 mg/mL solution of PbS QDs in octane (anhydrous, Sigma-Aldrich, 99+%) was spin-coated on ZnO films at 1500 rpm. Full exchange of 1,3-benzenedithiol (BDT) (Sigma-Aldrich, 99%) for the native oleic acid capping ligands was carried out by drop-casting a 1.7 mM solution of BDT in acetonitrile (anhydrous, Sigma-Aldrich, 99.8%) and waiting for 30 s before spin-drying. Films were then rinsed three times with acetonitrile to remove excess ligands. PbS QD and BDT solutions were dispensed through a 0.1 μm PTFE membrane filter. MoO$_3$ (Alfa Aesar, 99.9995%) and Au (Kurt J. Lesker, 3.175 mm pallets, 99.999%) were thermally evaporated through a shadow mask at 0.5 or 1.0 Å/s, respectively, at a base chamber pressure of 1 × 10^{-6} Torr. All fabrication steps were carried out in inert nitrogen atmosphere to prevent oxidation of the QDs and the ligands.

Device Characterization. Current−voltage characteristics of the PV devices were recorded in a nitrogen-filled glovebox using a computer-controlled Keithley 6487 picoammeter sourcemeter. 100 mW/cm^2 illumination was provided by a 150 W xenon arc lamp (Newport 96000) equipped with an AM 1.5G filter. The specular transmittance spectra of polymers were measured on quartz substrates with a Cary 5000 UV−vis-NIR dual-beam spectrophotometer. Sheet resistance was measured using a RM3-AR four point probe station from Jandel Engineering Ltd.

■ ASSOCIATED CONTENT

Ⓢ Supporting Information

Schematic diagram of the hydrothermal ZnO nanowire growth on graphene electrodes modified with conductive polymer interlayers; scanning electron microscopy (SEM) images of ZnO seed layer and ZnO nanowires grown on pristine graphene; SEM images of ZnO nanowires grown on spin-coated ZnO seed layer on ITO; SEM images of ZnO nanowires grown on a graphene/PEDOT:PEG(PC)/ZnO seed layer annealed at different temperatures. This material is available free of charge via the Internet at http://pubs.acs.org.

■ AUTHOR INFORMATION

Corresponding Author

*E-mail address: gradecak@mit.edu.

Author Contributions

⊥These authors contributed equally to this work.

■ REFERENCES

(1) Novoselov, K. S.; Jiang, D.; Schedin, F.; Booth, T. J.; Khotkevich, V. V.; Morozov, S. V.; Geim, A. K. *Proc. Natl. Acad. Sci. U. S. A.* **2005**, *102* (30), 10451−10453.

(2) Reina, A.; Jia, X. T.; Ho, J.; Nezich, D.; Son, H. B.; Bulovic, V.; Dresselhaus, M. S.; Kong, J. *Nano Lett.* **2009**, *9* (1), 30−35.

(3) Li, X. S.; Cai, W. W.; An, J. H.; Kim, S.; Nah, J.; Yang, D. X.; Piner, R.; Velamakanni, A.; Jung, I.; Tutuc, E.; Banerjee, S. K.; Colombo, L.; Ruoff, R. S. *Science* **2009**, *324* (5932), 1312−1314.

(4) Geim, A. K.; Novoselov, K. S. *Nature Mater.* **2007**, *6* (3), 183−191.

(5) Berger, C.; Song, Z. M.; Li, X. B.; Wu, X. S.; Brown, N.; Naud, C.; Mayou, D.; Li, T. B.; Hass, J.; Marchenkov, A. N.; Conrad, E. H.; First, P. N.; de Heer, W. A. *Science* **2006**, *312* (5777), 1191−1196.

(6) Bolotin, K. I.; Sikes, K. J.; Jiang, Z.; Klima, M.; Fudenberg, G.; Hone, J.; Kim, P.; Stormer, H. L. *Solid State Commun.* **2008**, *146* (9−10), 351−355.

(7) Wang, X. R.; Li, X. L.; Zhang, L.; Yoon, Y.; Weber, P. K.; Wang, H. L.; Guo, J.; Dai, H. J. *Science* **2009**, *324* (5928), 768−771.

(8) Bonaccorso, F.; Sun, Z.; Hasan, T.; Ferrari, A. C. *Nature Photonics* **2010**, *4* (9), 611−622.

(9) Park, H.; Brown, P. R.; Buloyic, V.; Kong, J. *Nano Lett.* **2012**, *12* (1), 133−140.

(10) De Arco, L. G.; Zhang, Y.; Schlenker, C. W.; Ryu, K.; Thompson, M. E.; Zhou, C. W. *Acs Nano* **2010**, *4* (5), 2865−2873.

(11) Wang, Y.; Tong, S. W.; Xu, X. F.; Ozyilmaz, B.; Loh, K. P. *Adv. Mater.* **2011**, *23* (13), 1514−1518.

(12) Han, T.; Lee, Y.; Choi, M.; Woo, S.; Bae, S.; Hong, B.; Ahn, J.; Lee, T. *Nature Photonics* **2012**, *6*, 105−110.

(13) Chung, K.; Lee, C.-H.; Yi, G.-C. *Science* **2010**, *330* (6004), 655−657.

(14) Bae, S.; Kim, H.; Lee, Y.; Xu, X. F.; Park, J.-S.; Zheng, Y.; Balakrishnan, J.; Lei, T.; Ri Kim, H.; Song, Y. I.; Kim, Y.-J.; Kim, K. S.; Ozyilmaz, B.; Ahn, J.-H.; Hong, B. H.; Iijima, S. *Nature Nanotechnol.* **2010**, *5* (8), 574−578.

(15) Savage, N. *Nature* **2012**, *483* (7389), S38−S39.

(16) Law, M.; Goldberger, J.; Yang, P. D. *Ann. Rev. Mater. Res.* **2004**, *34*, 83−122.

(17) Ren, S.; Zhao, N.; Crawford, S. C.; Tambe, M.; Bulović, V.; Gradečak, S. *Nano Lett.* **2010**, *11* (2), 408−413.

(18) Ren, S.; Chang, L.-Y.; Lim, S.-K.; Zhao, J.; Smith, M.; Zhao, N.; Bulović, V.; Bawendi, M. G.; Gradečak, S. *Nano Lett.* **2011**, *11* (9), 3998−4002.

(19) Kim, Y.-J.; Lee, J.-H.; Yi, G.-C. *Appl. Phys. Lett.* **2009**, *95* (21), 213101−3.

(20) Shin, K.-S.; Jo, H.; Shin, H.-J.; Choi, W. M.; Choi, J.-Y.; Kim, S.-W. *J. Mater. Chem.* **2012**, *22* (26), 13032−13038.

(21) Choi, W. M.; Shin, K. S.; Lee, H. S.; Choi, D.; Kim, K.; Shin, H. J.; Yoon, S. M.; Choi, J. Y.; Kim, S. W. *Nano Res.* **2011**, *4* (5), 440−447.

(22) Greene, L. E.; Law, M.; Tan, D. H.; Montano, M.; Goldberger, J.; Somorjai, G.; Yang, P. D. *Nano Lett.* **2005**, *5* (7), 1231−1236.

(23) Brewster, M. M.; Zhou, X.; Lu, M.-Y.; Gradečak, S. *Nanoscale* **2011**, *4* (5), 1455−1462.

(24) Ruankham, P.; Macaraig, L.; Sagawa, T.; Nakazumi, H.; Yoshikawa, S. *J. Phys. Chem. C* **2011**, *115* (48), 23809−23816.

(25) Munshi, A. M.; Dheeraj, D. L.; Fauske, V. T.; Kim, D.-C.; van Helvoort, A. T. J.; Fimland, B.-O.; Weman, H. *Nano Lett.* **2012**, *12* (9), 4570−4576.

(26) Wang, S. R.; Zhang, Y.; Abidi, N.; Cabrales, L. *Langmuir* **2009**, *25* (18), 11078−11081.

(27) Park, H.; Chang, S.; Smith, M.; Gradečak, S.; Kong, J. 2012, in preparation.

(28) Skotheim, T. A.; Reynolds, J. R., *Handbook of Conducting Polymers*; CRC press: Boca Raton, 2007.

(29) de Kok, M. M.; Buechel, M.; Vulto, S. I. E.; van de Weijer, P.; Meulenkamp, E. A.; de Winter, S.; Mank, A. J. G.; Vorstenbosch, H. J. M.; Weijtens, C. H. L.; van Elsbergen, V. *Phys. Status Solidi A* **2004**, *201* (6), 1342−1359.

(30) Chiu, W. W.; Travas-Sejdic, J.; Cooney, R. P.; Bowmaker, G. A. *J. Raman Spectrosc.* **2006**, *37* (12), 1354−1361.

(31) Sakamoto, S.; Okumura, M.; Zhao, Z.; Furukawa, Y. *Chem. Phys. Lett.* **2005**, *412* (4−6), 395−398.

(32) Jean, J.; Chang, S.; Brown, P. R.; Cheng, J. W. J.; Bawendi, M. G.; Gradečak, S.; Bulović, V., submitted for publication.

(33) Zhang, F.; Xu, X.; Tang, W.; Zhang, J.; Zhuo, Z.; Wang, J.; Wang, J.; Xu, Z.; Wang, Y. *Sol. Energy Mater. Sol. Cells* **2011**, *95* (7), 1785−1799.

(34) Olson, D. C.; Lee, Y.-J.; White, M. S.; Kopidakis, N.; Shaheen, S. E.; Ginley, D. S.; Voigt, J. A.; Hsu, J. W. P. *J. Phys. Chem. C* **2007**, *111* (44), 16640−16645.

(35) Yin, Z.; Wu, S.; Zhou, X.; Huang, X.; Zhang, Q.; Boey, F.; Zhang, H. *Small* **2010**, *6* (2), 307−312.

(36) Zhao, N.; Osedach, T. P.; Chang, L.-Y.; Geyer, S. M.; Wanger, D.; Binda, M. T.; Arango, A. C.; Bawendi, M. G.; Bulović, V. *ACS Nano* **2010**, *4* (7), 3743−3752.